Journal of Engineering Mathematics **33:** 31–46, 1998.

Onset of bouyancy-driven convection in superposed reacting fluid and porous layers

G. McKAY
Department of Mathematics, University of Strathclyde, 26 Richmond Street, Glasgow, G1 1XH, Scotland, U.K.

Received 23 October 1996; accepted in revised form 1 May 1997

Abstract. A linear stability analysis is applied to the onset of bouyancy-driven convection in a horizontal layer of reacting fluid overlying a porous region saturated with the same fluid. The fluid is assumed to be undergoing zero-order exothermic reactions in both regions. At the interface between fluid and porous layers the boundary conditions proposed by Nield [1] are employed; these include the empirical slip condition suggested by Beavers and Joseph [2].

Predictions for the onset of convection and critical wavenumbers are obtained from the analysis by the collocation method and solution of the resulting generalized eigenvalue problem. The effect of variable fluid/porous layer depth ratio, Frank–Kamenetskii number or thermal boundary conditions on the onset of fluid motions is studied, and ignition values of the Frank–Kamenetskii number for the system are calculated.

Key words: linear stability, Darcy's law, zero-order exothermic reaction, collocation method.

1. Introduction

The onset of convection in a layer of fluid overlying a porous region saturated with the fluid has many important applications in industry and geophysics. When a binary alloy is solidified directionally by cooling from below, a 'mushy zone' separating the melt from the solid may form (see, *e.g.*, Glicksman *et al.* [3]). This dendritic region is regarded as being a porous domain of variable permeability adjacent to a fluid layer. Following meltdown in a nuclear reactor, heat can be removed from solidified fuel particles by flooding the core with coolant (Schulenberg and Müller [4]). Mathematically this is modelled as a layer of fluid and one of saturated porous material. Similar fluid and porous interactions can model thermal storage systems and porous heat pipes. In geophysics flow within fluid and underlying porous layers has been presented by McKay and Straughan [5] in order to describe the generation of stone polygons on lake beds.

Several authors have investigated thermal instability in superposed fluid and saturated porous layers. Nield [1] considered a layered model and employed an empirical interfacial condition at the fluid/porous interface suggested by Beavers and Joseph [2]. The thermal stability for different systems of superposed porous and fluid regions has also been analyzed by Pillatsis *et al.* [6], and Taslim and Narusawa [7]. Chen and co-workers carried out experimental investigations and also studied the effects of salt-finger convection, throughflow and anisotropy in the porous matrix [8, 9, 10, 11].

Somerton and Catton [12] utilized the Brinkman extension to Darcy's law to analyze a two-layer region subject to constant volumetric heating. Similarly, in [4] simple interfacial conditions are employed in a study with constant internal heating. In many practical situations, however, constant heating within a fluid does not accurately describe the heat generated within the region, *e.g.*, fluids undergoing exothermic thermal reactions.

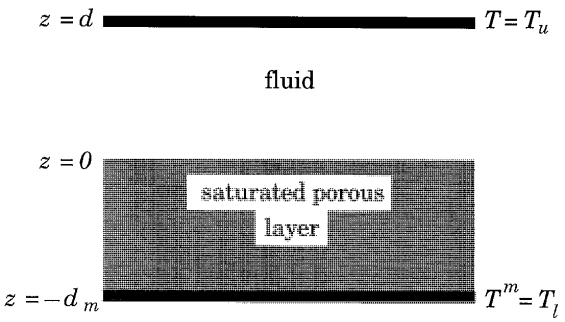

Figure 1. Two layer model.

The heat generated by a chemical reaction creates density differences in the fluid which can induce natural convection. Buoyancy-driven convection of reacting fluids within porous media occurs during oxidation of solid materials in large containers or the synthesis of ceramic materials. Furthermore, natural convection within porous media can remove heat from radioactive waste products waste products or delay the thermal explosion of coal piles or waste dumps. Therefore, the conditions for the onset of convection in a porous region are of great interest.

Jones [13] derived conditions for the onset of convection in an infinitely long region of reacting fluid. For a porous medium Kordylewski and Krajewski [14] considered natural convection based upon Darcy's law and assumed a zero-order exothermic reaction. Farr *et al.* [15] carried out a stability analysis for a similar convection problem, while Viljoen and Hlavacek [16] and Subramanian and Balakotaiah [17] solved the system numerically. Bifurcation studies of this type of convection have been carried out by Viljoen *et al.* [18], and Nandakumar and Weinitschke [19]. Malashetty *et al.* [20] also considered instability in a saturated porous region subject to cooling from above and different lower thermal conditions.

In this paper we examine the instability of a fluid layer overlying a saturated porous region and heated from below. We assume that the fluid is undergoing a zero-order exothermic reaction in both layers. Via a linear instability analysis we will obtain sufficient conditions for the onset of fluid motions in the system. These conditions are given as critical Rayleigh numbers for the fluid or for the porous region above which convection is guaranteed. We study the effect of variable layer thickness and thermal boundary conditions on the stability of the system. In addition we calculate ignition conditions for the system and investigate the influence of chemical heating, permeability or porosity on the stability of the fluid.

2. Model

We shall suppose that the reacting fluid occupies the infinite layer between $z = 0$ and $z = d$. Underlying is a region of fluid and porous material between $z = -d_m$ and $z = 0$ (see Figure 1). We shall assume the inert porous matrix to be homogeneous, saturated and in local thermal equilibrium with the chemically reacting fluid. The region is cooled from above with the upper boundary $z = d$ kept at a constant temperature of $T = T_u$, where T is the fluid temperature. We assume that the temperature of the whole domain varies only slightly from T_u so that a zero-order reaction can be assumed. Throughout a sub- or super-script m denotes a variable for the porous layer.

In the fluid layer $z \in (0, d)$ we have a linear viscous, incompressible fluid. Employing the Boussinesq approximation, we obtain the equations of motion

$$\rho_0(u_{i,t} + u_j u_{i,j}) = -p_{,i} + \mu u_{i,jj} - \rho_0 g k_i[1 - \beta(T - T_u)], \tag{1}$$

$$u_{i,i} = 0, \tag{2}$$

$$T_{,t} + u_i T_{,i} = \frac{k_f}{(\rho_0 C_0)_f} T_{,jj} + Q \exp\left(-\frac{E}{RT}\right), \tag{3}$$

where $\boldsymbol{u}, T, p, t, \mu, g, k_f, \rho_0, \beta, C_0$ are, respectively, fluid velocity, temperature, pressure, time, dynamic viscosity, gravity constant, thermal conductivity, fluid density, thermal expansion coefficient and specific heat. Further, $(\rho_0 C_0)_f$ is the thermal capacitance for the fluid. Standard indicial notation has been employed with $\boldsymbol{k} = (0, 0, 1)$. The final term in (3) represents the heat generated by the reacting fluid. Also, E is the activation energy, R the universal gas constant and Q is the product of the heat of reaction, reactant concentration and a pre-exponential factor. In general, the reactant concentration is variable; however, in this study attention is restricted to a zero-order reaction in the fluid where only a negligible amount of reactant is depleted (*i.e.* Q is assumed to be constant).

In the porous media $z \in (-d_m, 0)$ the equations of motion we adopt are based upon Darcy's law and the Boussinesq approximation (see Nield and Bejan [21]). The equations of momentum, continuity and energy for the porous layer are

$$\frac{\rho_0}{\phi} u^m_{i,t} = -p^m_{,i} - \rho_0 g k_i[1 - \beta(T^m - T_u)] - \frac{\mu}{k'} u^m_i, \tag{4}$$

$$u^m_{i,i} = 0, \tag{5}$$

$$\frac{(\rho_0 C_0)_m}{(\rho_0 C_0)_f} T^m_{,t} + u^m_i T^m_{,i} = \frac{k_m}{(\rho_0 C_0)_f} T^m_{,jj} + \phi Q \exp\left(-\frac{E}{RT^m}\right). \tag{6}$$

Here, $\boldsymbol{u}^m, T^m, p^m, k', \phi$ are fluid seepage velocity in the porous region, temperature, pressure, permeability, and porosity, respectively. The parameters k_m and $(\rho_0 C_0)_m$ are the *effective* thermal conductivity and capacitance for the region, *i.e.*, if k_f and k_s are the thermal conductivities for the fluid and the porous matrix, respectively, then

$$k_m = \phi k_f + (1 - \phi) k_s.$$

Finally, we observe that the final heat source term in (6) is pre-multiplied by porosity to take into account the porous nature of the lower region; less heat is produced per unit volume in the lower region owing to the presence of inert porous material.

For boundary conditions we assume the fluid surface to be rigid, *i.e.*

$$z = d: \qquad T = T_u, \qquad u_3 = \frac{\partial u_3}{\partial z} = 0. \tag{7}$$

On the lower boundary of the porous region we assume that the bounding wall is isothermal and rigid

$$z = -d_m: \qquad T^m = T_l, \qquad u^m_3 = 0, \tag{8}$$

where $T_l > T_u$. The boundary conditions at the interface $z = 0$ guarantee continuity of normal velocity, temperature, heat flux and normal stress

$$\begin{aligned} &z = 0\text{:} \qquad u_3 = u_3^m, \qquad -p + 2\mu\frac{\partial u_3}{\partial z} = -p^m, \\ &T = T^m = T_0, \qquad k_f\frac{\partial T}{\partial z} = k_m\frac{\partial T^m}{\partial z}, \end{aligned} \tag{9}$$

where the interface temperature T_0 is to be determined. For the remaining condition at the interface we follow Nield [1] who uses the empirical relation suggested by Beavers and Joseph [2]. This relation relates slip velocity to flow in the fluid via

$$\frac{\partial u_1}{\partial z} = \frac{\alpha^*}{\sqrt{k'}}\left(u_1 - u_1^m\right), \qquad \frac{\partial u_2}{\partial z} = \frac{\alpha^*}{\sqrt{k'}}\left(u_2 - u_2^m\right), \tag{10}$$

where $\partial/\partial z$ denotes the derivative as $z \to 0^+$ and α^* is a dimensionless quantity depending on the physical properties of the porous material. Beavers and Joseph [2] based their law on experimental evidence using three types of Foametal and two types of Aloxite for porous media. For these materials k' and α^* have values ranging from $k' = 9{\cdot}7 \times 10^{-9}$ (m^2) to $8{\cdot}2 \times 10^{-8}$ and $\alpha^* = 0{\cdot}78$ to 4 for Foametal, and $k' = 6{\cdot}5 \times 10^{-10}$ (m^2) to $1{\cdot}6 \times 10^{-9}$ and $\alpha^* = 0{\cdot}1$ for Aloxite. Theoretical and experimental investigations have provided support for this condition (see, *e.g.*, Neale and Nader [22], Beavers *et al.* [23]). As remarked in Chen and Chen [9], results are insensitive to variations in α^* which is set to unity in this analysis. Jones [24] offers an alternative condition involving shear stress rather than just velocity shear. However in McKay and Straughan [5] it was shown that the extra terms introduced by the shear stress relation had only a minimal effect. Attention here is restricted to the simpler boundary condition (10).

Equations (1)–(3) possess a z-dependent conduction solution $(\bar{\boldsymbol{u}}, \bar{p}, T_u + T_r\bar{\Theta})$ and (4)–(6) are satisfied by $(\bar{\boldsymbol{u}}^m, \bar{p}^m, T_u + T_r\bar{\Theta}^m)$, where the reference temperature for the reacting fluid $T_r = RT_u^2/E$ and

$$\bar{\boldsymbol{u}} = \boldsymbol{0}, \qquad \bar{\boldsymbol{u}}^m = \boldsymbol{0},$$

$$\frac{\mathrm{d}\bar{p}}{\mathrm{d}z} = -\rho_0 g[1 - \beta T_r\bar{\Theta}], \qquad \frac{\mathrm{d}\bar{p}^m}{\mathrm{d}z} = -\rho_0 g[1 - \beta T_r\bar{\Theta}^m],$$

$$T_r k_f\frac{\mathrm{d}^2\bar{\Theta}}{\mathrm{d}z^2} = -(\rho_0 C_0)_f Q\,\exp\left(-\frac{E}{R(T_u + T_r\bar{\Theta})}\right), \tag{11}$$

$$T_r k_m\frac{\mathrm{d}^2\bar{\Theta}^m}{\mathrm{d}z^2} = -\phi(\rho_0 C_0)_f Q\,\exp\left(-\frac{E}{R(T_u + T_r\bar{\Theta}^m)}\right). \tag{12}$$

Equations (11)–(12) are solved subject to boundary conditions

$$\begin{aligned} &z = d\text{:} \qquad \bar{\Theta} = 0, \\ &z = 0\text{:} \qquad k_f\frac{\mathrm{d}\bar{\Theta}}{\mathrm{d}z} = k_m\frac{\mathrm{d}\bar{\Theta}^m}{\mathrm{d}z}, \qquad \bar{\Theta} = \bar{\Theta}^m = \frac{T_0 - T_u}{T_r} = \Theta_0, \end{aligned} \tag{13}$$

$$z = -d_m \qquad \bar{\Theta}^m = \frac{T_l - T_u}{T_r} = \Theta_l,$$

with Θ_0 and Θ_l defined as indicated. Assuming $RT_u/E = T_r/T_u \ll 1$, we may rewrite the exponent in (11) as

$$\exp\left(-\frac{E}{R(T_u + T_r\bar{\Theta})}\right) = \exp\left(-\frac{E}{RT_u}\right)\ \exp(\bar{\Theta}),$$

with a similar expression for (12)

Introducing the variables

$$\hat{d} = \frac{d_m}{d}, \qquad \hat{k} = \frac{k_m}{k_f}, \qquad \delta = \frac{Q(\rho_0 C_0)_f d^2}{T_r k_f}\ \exp\left(-\frac{E}{RT_u}\right),$$

where δ is the Frank–Kamenetskii number, we obtain by integration of (11) and (12) solutions

$$\delta = 0\text{:} \qquad \bar{\Theta} = \Theta_0\left(1 - \frac{z}{d}\right), \qquad \bar{\Theta}^m = \Theta_0\left(1 - \frac{z}{d\hat{k}}\right),$$

$$\delta \neq 0\text{:} \qquad \exp(\bar{\Theta}) = \frac{c_1}{2\delta}\left(1 - \left(\frac{1 - c_2\ \exp(-\sqrt{c_1}z/d)}{1 + c_2\ \exp(-\sqrt{c_1}z/d)}\right)^2\right), \tag{14}$$

$$\exp(\bar{\Theta}^m) = \frac{c_3}{2\delta^*}\left(1 - \left(\frac{1 - c_4\ \exp(-\sqrt{c_3}z/d)}{1 + c_4\ \exp(-\sqrt{c_3}z/d)}\right)^2\right),$$

where

$$\delta^* = \frac{\phi\delta}{\hat{k}}.$$

Here c_1, c_2, c_3, c_4 are constants of integration, while the non-dimensional interface temperature Θ_0 is also determined by the boundary conditions. Indeed, when $\delta = 0$, we can show that

$$\Theta_0 = \frac{\Theta_l}{1 + \hat{d}/\hat{k}}. \tag{15}$$

When $\delta \neq 0$, we substitute (13) in (14) to determine the constants of integration and Θ_0 via

$$1 = \frac{c_1}{2\delta}\left(1 - \left(\frac{1 - c_2\ \exp(-\sqrt{c_1})}{1 + c_2\ \exp(-\sqrt{c_1})}\right)^2\right),$$

$$\exp(\Theta_l) = \frac{c_3}{2\delta^*}\left(1 - \left(\frac{1 - c_4\ \exp(-\sqrt{c_3}\hat{d})}{1 + c_4\ \exp(-\sqrt{c_3}\hat{d})}\right)^2\right),$$

$$\exp(\Theta_0) = \frac{c_1}{2\delta}\left(1 - \left(\frac{1 - c_2}{1 + c_2}\right)^2\right) = \frac{c_3}{2\delta^*}\left(1 - \left(\frac{1 - c_4}{1 + c_4}\right)^2\right), \tag{16}$$

$$k_f\sqrt{c_1 - 2\delta\ \exp(\Theta_0)} = k_m\sqrt{c_3 - 2\delta^*\ \exp(\Theta_0)}.$$

When $d_m = 0$ or $d = 0$ (*i.e.* only one region of reacting fluid) we can solve (16) explicitly for c_1 and c_2, or c_3 and c_4. However, in this study we restrict attention to $0{\cdot}001 \leqslant \hat{d} \leqslant 100$; therefore we find the values of c_1, c_2, c_3, c_4 and Θ_0 numerically.

Ignition begins in the system when the heat generated by the reacting fluid is high enough to support further reactions without continual heat transfer from the lower boundary wall. At this critical point there is no longer a stream of heat entering the system; therefore the heat transported by convection is due entirely to the chemical reaction's internal heating. The ignition point corresponds to adiabatic conditions at the lower boundary

$$\frac{\mathrm{d}\Theta^m}{\mathrm{d}z}(-d_m) = 0. \tag{17}$$

Applying (17) to $(14)_4$ we obtain the ignition condition

$$\delta_c = \frac{c_3\hat{k}}{2\phi}\ \exp(-\Theta_l), \tag{18}$$

where δ_c is the critical (or ignition) Frank–Kamenetskii number beyond which the reaction in the fluid is self-sustainable and the nature of the lower boundary condition changes. We consider only Frank–Kamenetskii numbers below the critical value.

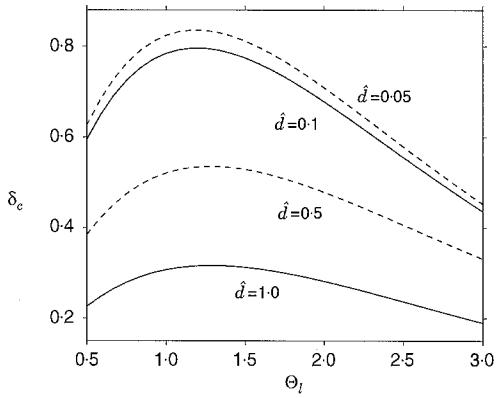

Figure 2. The effect of the lower boundary thermal condition on ignition Frank–Kamenetskii number; $\hat{k} = 0{\cdot}5,\ \ \phi = 0{\cdot}5$.

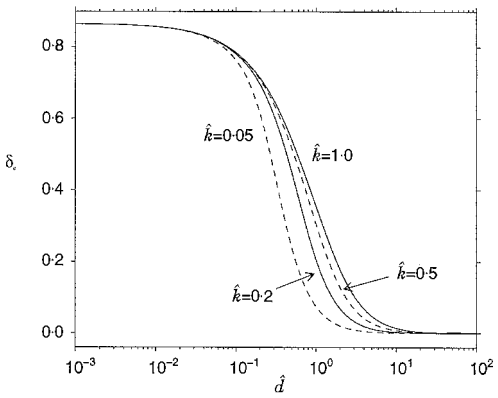

Figure 3. Variation of ignition Frank–Kamenetskii number with depth ratio and thermal conductivity ratio; $\Theta_l = 1{\cdot}0,\ \ \phi = 0{\cdot}5$.

In Figures 2, 3 we have computed critical Frank–Kamenetskii numbers for variable Θ_l, $\hat{d}$ and $\hat{k}$. In Figure 2, δ_c obtains a finite maximum as Θ_l is increased from 0 before monotonically decreasing. For a single fluid layer $(\hat{d} = 0)$ Malashetty *et al.* [20] calculate a maximum δ_c of $0{\cdot}8785$ at $\Theta_l = 1{\cdot}19$. For the data considered in this two layer problem a maximum δ_c also occurs at approximately $\Theta_l = 1{\cdot}20$, even when the relative layer depths are allowed to vary.

If we allow the porous layer thickness, d_m, to increase, while the fluid depth, d, is constant, the overall thickness of the system and $\hat{d}$ also increase. For fixed thermal boundary conditions the increase in d_m results in a decrease in the magnitude of the temperature gradients across the system. The adiabatic condition for ignition can therefore be achieved for smaller values

of the Frank–Kamenetskii number. In Figure 3 we observe that the decrease in δ_c is most dramatic for $0{\cdot}1 < \hat{d} < 10$. The Frank–Kamenetskii number is defined as a function of d^2, so that $\delta_c \to 0$ as $\hat{d} \to \infty$. When the porous region is much thicker than the fluid layer, we can obtain more information by defining a new Frank–Kamenetskii number related to the *porous-layer thickness*. As $\hat{d} \to 0, \delta_c$ approaches a constant limiting value. This limit is independent of the ratio of conductivities; however, there is a variation with Θ_l. From Figure 3 it can also be seen that variation of the relative thermal conductivities has only a small effect on the critical Frank–Kamenetskii number.

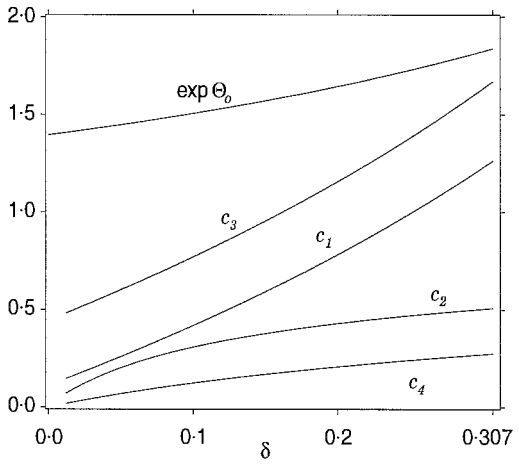

Figure 4. Constants of integration for variable Frank–Kamenetskii number; $\hat{d} = 1{\cdot}0$, $\Theta_l = 1{\cdot}0$, $\hat{k} = 0{\cdot}5$, $\phi = 0{\cdot}5$, $\delta_c = 0{\cdot}307$.

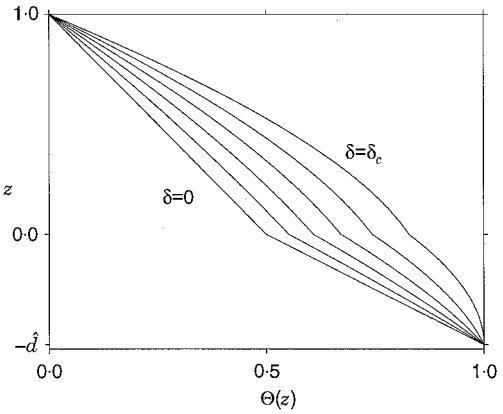

Figure 5. Steady temperature profiles. Frank–Kamenetskii number takes values $\delta = (i/5)\delta_c$, $i = 0, \ldots, 5$; $\hat{d} = 0{\cdot}5$, $\Theta_l = 1{\cdot}0$, $\hat{k} = 0{\cdot}5$, $\phi = 0{\cdot}5$, $\delta_c = 0{\cdot}520$.

From Figure 4 observe that the constants of integration and non-dimensional interfacial temperature Θ_0 all increase as δ approaches its ignition value. We can extrapolate the plot for $\exp(\Theta_0)$ back to the result for $\delta = 0$ by using (15). Undisturbed temperature profiles as a function of the vertical ordinate are given in Figure 5 for different values of δ. When $\delta = 0$, the profiles are piecewise linear, the different gradients result from the different thermal conductivities in each region ($\hat{k} = 0{\cdot}5$). For δ small the profiles remain piecewise linear. However, as δ increases the heat generated due to the chemical reaction also increases. This gives rise to nonlinear basic profiles.

3. Linear stability analysis

We perform a linear stability analysis by introducing perturbations to the steady solution via

$$\begin{aligned} &\boldsymbol{u} = \bar{\boldsymbol{u}} + \boldsymbol{v}, \qquad p = \bar{p} + \pi, \qquad T = T_u + T_r\bar{\Theta} + \theta, \\ &\boldsymbol{u}^m = \bar{\boldsymbol{u}}^m + \boldsymbol{v}^m, \qquad p^m = \bar{p}^m + \pi^m, \qquad T^m = T_u + T_r\bar{\Theta}^m + \theta^m. \end{aligned} \tag{19}$$

Substituting (19) in (1)–(6), we non-dimensionalize the perturbation equations with the scalings

$$z \in (0, d): \qquad z = dz^*, \qquad t = T^* t^*, \qquad \boldsymbol{v} = V\boldsymbol{v}^*,$$

$$\theta = T^{\#}\theta^*, \qquad \pi = P\pi^*, \qquad T^* = \frac{d^2\rho_0}{\mu},$$

$$V = \frac{\mu}{d\rho_0}, \qquad T^{\#} = \frac{T_r V d\xi(\rho_0 C_0)_f}{k_f}, \qquad P = \frac{\mu^2}{d^2\rho_0},$$

$$z \in (-d_m, 0): \qquad z = d_m z^*, \qquad t = T^{*m} t^*, \qquad \boldsymbol{v}^m = V^m \boldsymbol{v}^{*m},$$

$$\theta^m = T^{\#m}\theta^{*m}, \qquad \pi^m = P^m \pi^{*m}, \qquad T^{*m} = \frac{d_m^2\rho_0}{\mu},$$

$$V^m = \frac{\mu\hat{k}}{d_m\rho_0}, \qquad T^{\#m} = \frac{\hat{d}T^{\#}}{\hat{k}}, \qquad P^m = \frac{\mu V^m d_m}{k'}$$

and by introducing dimensionless numbers

$$Da = \frac{k'}{d_m^2}, \qquad A = \frac{Da}{\phi}, \qquad \xi = \frac{\Theta_l}{1+\hat{d}/\hat{k}}, \qquad \gamma = \frac{(\rho_0 C_0)_m}{(\rho_0 C_0)_f}, \qquad Pr = \frac{\mu(\rho_0 C_0)_f}{\rho_0 k_f},$$

$$Ra = \frac{gd^3\beta T_r \xi \rho_0 (\rho_0 C_0)_f}{k_f \mu}, \qquad Ra_m = \frac{Da\,\hat{d}^4}{\hat{k}^2} Ra.$$

Here, Ra is the Rayleigh number for the fluid region while Ra_m is the Rayleigh number for the porous region. Da is the Darcy number for the porous matrix, Pr is the Prandtl number for the fluid, A is the non-dimensional acceleration coefficient, and γ is the ratio of thermal capacities for the two layers. Finally, ξ is the non-dimensional interface temperature we expect between the porous and fluid layers when $\delta = 0$.

The linearized non-dimensional perturbation equations are then (stars omitted)

$$v_{i,t} = -\pi_{,i} + v_{i,jj} + Ra\theta k_i, \tag{20}$$

$$v_{i,i} = 0, \tag{21}$$

$$Pr\theta_{,t} = -\left[\frac{d}{\xi}\frac{\mathrm{d}\bar{\Theta}}{\mathrm{d}z}\right] w + \theta_{,jj} + \delta\, \exp(\bar{\Theta})\theta, \tag{22}$$

for $z \in (0, 1)$, and

$$Av^m_{i,t} = -\pi^m_{,i} - v^m_i + Ra_m\theta^m k_i, \tag{23}$$

$$v^m_{i,i} = 0, \tag{24}$$

$$Pr\frac{\gamma}{\hat{k}}\theta^m_{,t} = -\left[\frac{\hat{k}d}{\xi}\frac{\mathrm{d}\bar{\Theta}^m}{\mathrm{d}z}\right] w^m + \theta^m_{,jj} + \delta^*\hat{d}^2\, \exp(\bar{\Theta}^m)\theta^m, \tag{25}$$

for $z \in (-1, 0)$, where $\boldsymbol{v} = (u, v, w)$ and $\boldsymbol{v}^m = (u^m, v^m, w^m)$. The boundary conditions on the perturbation variables become

$$z = 1: \qquad w = \frac{\partial w}{\partial z} = 0, \qquad \theta = 0, \tag{26}$$

$$z = -1: \qquad w^m = 0, \qquad \theta^m = 0. \tag{27}$$

The interface boundary conditions for the non-dimensionalized variables are now

$$z = 0: \qquad w = \frac{\hat{k}}{\hat{d}} w^m, \qquad \theta = \frac{\hat{d}}{\hat{k}} \theta^m, \qquad \frac{\partial \theta}{\partial z} = \frac{\partial \theta^m}{\partial z}, \tag{28}$$

$$-\pi + 2\frac{\partial w}{\partial z} = -\frac{\hat{k}}{Da\,\hat{d}^2} \pi^m, \tag{29}$$

$$\frac{\partial u}{\partial z} = \frac{\alpha^*}{\sqrt{Da}\,\hat{d}} \left(u - \frac{\hat{k}}{\hat{d}} u^m \right), \tag{30}$$

$$\frac{\partial v}{\partial z} = \frac{\alpha^*}{\sqrt{Da}\,\hat{d}} \left(v - \frac{\hat{k}}{\hat{d}} v^m \right). \tag{31}$$

Differentiating (30) with respect to x, (31) with respect to y and utilizing (21) and (24), we can derive the following condition for the third components of the velocities

$$\frac{\hat{d}^3 \sqrt{Da}}{\alpha^*} \frac{\partial^2 w}{\partial z^2} - \hat{d}^2 \frac{\partial w}{\partial z} + \hat{k} \frac{\partial w^m}{\partial z} = 0. \tag{32}$$

And in a similar approach we can obtain a single boundary condition from (29)

$$\frac{\partial^3 w}{\partial z^3} + 3\Delta^* \frac{\partial w}{\partial z} + \frac{\hat{k}}{Da\,\hat{d}^4} \frac{\partial w^m}{\partial z} - \frac{\partial^2 w}{\partial z \partial t} + \frac{A\hat{k}}{Da\,\hat{d}^4} \frac{\partial^2 w^m}{\partial z \partial t} = 0, \tag{33}$$

where $\Delta^* = \partial^2/\partial x^2 + \partial^2/\partial y^2$. The derivation of (32)–(33) is very similar to the analysis in Nield [1].

We now take the third components of curl curl (20) and (23), then expand our variables in normal mode form

$$(w, \theta) = (W(z), \vartheta(z)) \ \exp(\sigma t) \Phi(x, y),$$

$$(w^m, \theta^m) = (W^m(z), \vartheta^m(z)) \ \exp(\sigma_m t) \Phi^m(x, y).$$

Planforms $\Phi(x, y)$ and $\Phi^m(x, y)$ are chosen such that

$$\Delta^* \Phi = -\alpha^2 \Phi, \qquad \Delta^* \Phi^m = -\alpha_m^2 \Phi^m,$$

where α and α_m are the wavenumbers for the fluid region and the porous region, respectively. It follows from the non-dimensionalization that these wavenumbers are related via

$$\frac{\alpha_m}{\alpha} = \hat{d}. \tag{34}$$

Similarly, the time-scales for the fluid and porous layers have been scaled differently, so the growth rates σ and σ_m are related via

$$\frac{\sigma_m}{\sigma} = \hat{d}^2. \tag{35}$$

Employing normal modes, we see that the linearized equations become

$$\begin{aligned}&(D^4 - 2\alpha^2 D^2 + \alpha^4)W - \alpha^2 Ra\,\vartheta - \sigma(D^2 - \alpha^2)W = 0,\\&(D^2 - \alpha^2 + \delta\,\exp(\bar{\Theta}))\vartheta - \left[\frac{d}{\xi} D\bar{\Theta}\right] W - \sigma Pr\vartheta = 0,\end{aligned} \tag{36}$$

for $z \in (0, 1)$; and

$$\begin{aligned}&(D^2 - \alpha_m^2)W^m + \alpha_m^2 Ra_m \vartheta^m + \sigma_m A(D^2 - \alpha_m^2)W^m = 0,\\&(D^2 - \alpha_m^2 + \hat{d}^2\delta^*\,\exp(\bar{\Theta}))\vartheta - \left[\frac{d\hat{k}}{\xi} D\bar{\Theta}^m\right] W^m - \sigma_m Pr\frac{\gamma}{\hat{k}}\vartheta^m = 0,\end{aligned} \tag{37}$$

for $z \in (-1, 0)$, where $D = \mathrm{d}/\mathrm{d}z$. The boundary conditions become

$$\begin{aligned}&z = 1: \qquad W = DW = 0, \qquad \vartheta = 0,\\&z = -1: \qquad W^m = 0, \qquad \vartheta^m = 0,\\&z = 0: \qquad W = \frac{\hat{k}}{\hat{d}} W^m, \qquad \vartheta = \frac{\hat{d}}{\hat{k}}\vartheta^m, \qquad D\vartheta = D\vartheta^m,\\&\frac{\hat{d}^3\sqrt{Da}}{\alpha^*} D^2 W - \hat{d}^2 DW + \hat{k}W^m = 0,\\&D^3 W - 3\alpha^2 DW + \frac{\hat{k}}{Da\,\hat{d}^4} DW^m - \sigma DW + \sigma_m \frac{A\hat{k}}{Da\,\hat{d}^4} DW^m = 0.\end{aligned} \tag{38}$$

Conditions for the onset of convection in the two layers are obtained from (36)–(38); they define a characteristic problem for σ (or σ_m which is related to σ via (35)). For fixed boundary conditions and given values of (Ra, α) solutions to (36)–(38) can be found only for discrete values of σ (or σ_m). Since we are interested in the onset of stationary or oscillatory convection, we seek critical Rayleigh numbers and wavenumbers for which $\sigma(Ra, \alpha)$ is an eigenvalue of our system and

$$\mathrm{Re}(\sigma(Ra, \alpha)) = 0. \tag{39}$$

The *critical Rayleigh number* for the fluid/porous system, Ra_c, is the minimum Rayleigh number for which there exists an eigenvalue satisfying (39). The *critical wavenumber* at which this minimum occurs is α_c. Alternatively, depending on the relative depth of the fluid and saturated porous layers, we sometimes employ critical numbers for the porous region

$$Ra_{mc} = \frac{Da\,\hat{d}^4}{\hat{k}^2} Ra_c, \qquad \alpha_{mc} = \hat{d}\alpha_c.$$

Critical Rayleigh numbers Ra_c or Ra_{mc} represent a boundary for instability. When the Rayleigh number and wavenumber of our system obtain their critical values, $\mathrm{Re}(\sigma)$ changes sign from negative to positive and fluid motions are guaranteed. If at the critical point $\mathrm{Im}(\sigma) = 0$, then exchange of stabilities holds and stationary convection occurs. Otherwise the motions

in the layers are oscillatory. It is known that exchange of stabilities holds for convection in a fluid layer, or in a saturated porous layer.

To obtain characteristic values from (36)–(38), we employ the collocation method (Boyd [25]). First, we transform our regions $z \in (0,1)$ and $z \in (-1,0)$ into two domains over $z_n \in (-1,1)$ via

$$z \in (0,1): \qquad z_n = 1 - 2z; \qquad z \in (-1,0): \qquad z_n = 2z + 1.$$

In doing so, we now obtain a tenth-order system of equations on the domain $z_n \in (-1,1)$: one fourth-order differential equation and three second-order equations. The upper and lower boundaries of our original two layer problem now coincide at $z_n = -1$, while our interface between regions corresponds to $z_n = 1$.

Next we discretize our domain $z_n \in (-1,1)$ into N-subintervals via Chebyshev nodes

$$x_i = -\cos\frac{i\pi}{N}, \qquad i = 0, \ldots, N.$$

For the collocation method the solution $W(z_n)$ is expanded in a series of Chebyshev polynomials, *i.e.*

$$W(z_n) = \sum_{j=0}^{N} c_j T_j(z_n), \tag{40}$$

where c_j are constant coefficients. The value of $W(z_n)$ at each node is given by

$$w_i = W(x_i) = \sum_{j=0}^{N} c_j T_j(x_i), \qquad i = 0, \ldots, N. \tag{41}$$

The derivative of $W(z_n)$ can also be expanded in a similar manner

$$W'(z_n) = \sum_{j=0}^{N} b_j T_j(z_n),$$

from which we can obtain the derivative at each node point

$$\begin{aligned} w_i' = W'(x_i) &= \sum_{j=0}^{N} b_j T_j(x_i) \\ &= \sum_{j=0}^{N} d_{ij} w_j, \qquad i = 0, \ldots, N. \end{aligned}$$

The vector $\boldsymbol{w}' = (w_0', \ldots, w_N')^T$ can now be written as

$$\boldsymbol{w}' = \mathcal{D}\boldsymbol{w},$$

where $\boldsymbol{w} = (w_0, \ldots, w_N)^T$ and $\mathcal{D} = (d_{ij})$ is a first-order differentiation matrix on $N+1$ nodes. A similar procedure can be carried out for $W^m(z_n)$, $\vartheta(z_n)$ and $\vartheta^m(z_n)$.

In the collocation method we require that (36) and (37) are satisfied *at the node points* $x_i, i = 0, \ldots, N$. If $\mathcal{D}^k$ represents the kth-order differentiation matrix for $k = 2$ and 4, we obtain by substituting $z_n = x_i$ $(i = 0, \ldots, N)$ in system (36)–(37)

$$\begin{pmatrix} \mathcal{D}^4 - 2\alpha^2\mathcal{D}^2 + \alpha^4\,\mathrm{I} & -\alpha^2 Ra\,\mathrm{I} & 0 & 0 \\ \mathrm{N} & \mathcal{D}^2 - \alpha^2\,\mathrm{I} + \mathrm{M} & 0 & 0 \\ 0 & 0 & \mathcal{D}^2 - \alpha_m^2\,\mathrm{I} & \alpha_m^2 Ra_m\,\mathrm{I} \\ 0 & 0 & \mathrm{N}_m & \mathcal{D}^2 - \alpha_m^2\,\mathrm{I} + \mathrm{M}_m \end{pmatrix} \begin{pmatrix} \boldsymbol{w} \\ \boldsymbol{\vartheta} \\ \boldsymbol{w}^m \\ \boldsymbol{\vartheta}^m \end{pmatrix}$$

$$- \sigma \begin{pmatrix} \mathcal{D}^2 - \alpha^2\,\mathrm{I} & 0 & 0 & 0 \\ 0 & Pr\,\mathrm{I} & 0 & 0 \\ 0 & 0 & -A\hat{d}^2(\mathcal{D}^2 - \alpha_m^2\,\mathrm{I}) & 0 \\ 0 & 0 & 0 & Pr\gamma(\hat{d}^2/\hat{k})\,\mathrm{I} \end{pmatrix} \begin{pmatrix} \boldsymbol{w} \\ \boldsymbol{\vartheta} \\ \boldsymbol{w}^m \\ \boldsymbol{\vartheta}^m \end{pmatrix} = \begin{pmatrix} 0 \\ 0 \\ 0 \\ 0 \end{pmatrix}, \quad (42)$$

where $\boldsymbol{w}^m$, $\boldsymbol{\vartheta}$ and $\boldsymbol{\vartheta}^m$ are the vectors of function values at node points. I is the $(N+1)\times(N+1)$ identity matrix. M and N are the diagonal matrices representing $\delta\,\exp(\bar{\Theta})$ and $-(d/\xi)\,\mathrm{d}\bar{\Theta}/\mathrm{d}z$ at node points (with similar definitions for M_m and N_m).

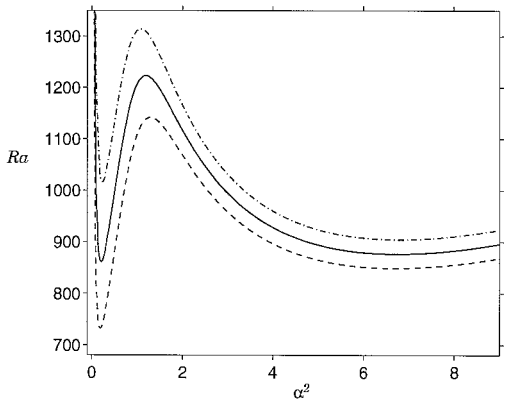

Figure 6. Marginal stability curves for different ratios $\hat{d}$; $(- \cdot -\cdot)$: $\hat{d} = 4{\cdot}5$, (—): $\hat{d} = 4{\cdot}7$, $(- - -)$: $\hat{d} = 4{\cdot}9$; $\Theta_l = 1{\cdot}0$, $\hat{k} = 0{\cdot}5$, $\phi = 0{\cdot}5$, $Da = 10^{-5}$, $\delta = 0{\cdot}02$.

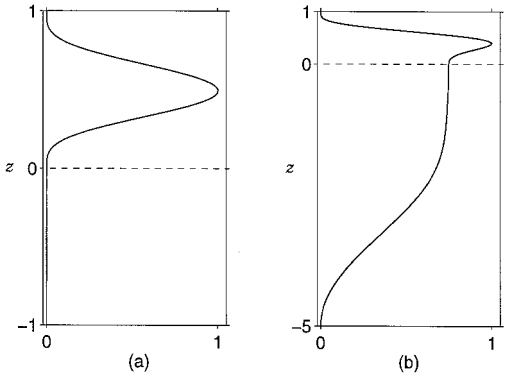

Figure 7. Normalized vertical velocity components; (a): $\hat{d} = 1$, (b): $\hat{d} = 5$; $\Theta_l = 1{\cdot}0$, $\hat{k} = 0{\cdot}5$, $\phi = 0{\cdot}5$, $Da = 10^{-4}$, $\delta = 0{\cdot}02$.

A collocation method is favoured here because of the presence of nonlinear coefficients in (36) and (37). For spectral methods (*e.g.* Chebyshev–Tau methods) we require to calcuate the inner product of $\exp(\bar{\Theta})$ or $\mathrm{d}\bar{\Theta}/\mathrm{d}z$ with some trial function. The collocation method is simpler as we need only calculate $\exp(\bar{\Theta})$ or $\mathrm{d}\bar{\Theta}/\mathrm{d}z$ at the node points, thus greatly reducing processor time.

Finally, we incorporate the boundary conditions at $z_n = 1$ or $z_n = -1$. The zero boundary conditions for $W, W^m, \vartheta, \vartheta^m$ at $z_n = -1$ reduce our matrix equation to a $4N \times 4N$ generalized eigenvalue problem for σ and a reduced eigenvector $(\boldsymbol{w}, \boldsymbol{\vartheta}, \boldsymbol{w}^m, \boldsymbol{\vartheta}^m)^T$. The reduced eigenvector no longer includes function values at node point $x_0 = -1$. The eigenvalues are

obtained via the QZ algorithm of Moler and Stewart [26], and $W(z_n)$ can then be determined from (41).

Since we require to find only the eigenvalue of system (42) closest to zero, there is little variation in our results for different N. When $N = 25$ and $N = 50$, our critical numbers in general vary by no more than 0·5 percent; so in the following we have fixed the number of intervals to be $N = 25$. For all the data considered here we find that $\mathrm{Im}(\sigma) = 0$ at the critical point, *i.e.*, exchange of stabilities holds and any disturbances grow with time monotonically. Therefore in Section 4 our critical conditions for instability are independent of Pr, A and γ.

4. Results

Marginal stability curves given in Figure 6 represent values of (Ra, α^2) for which there exist eigenvalues $\sigma(Ra, \alpha^2)$ satisfying (39). The curves are bimodal, similar to those in Chen and Chen [9] for superposed layers without heat generation. For the data considered, when $\hat{d} < 4{\cdot}7$ it can be seen that the critical (or minimum) Rayleigh number in on the short-wave branch of the curve. This critical point corresponds to the onset of convection dominated by motions in the fluid layer. For $\hat{d} > 4{\cdot}7$, motions are concentrated in the porous region, characterized by a longer wavelength. Whenever we express results for this regime, we employ the critical numbers Ra_{mc} and a_{mc}.

To demonstrate this bimodal nature, in Figure 7 we have plotted vertical velocity components for the original domain $z \in (-\hat{d}, 1)$ at *the onset of convection*, continuous at the interface and normalized to have a unit maximum. When $\hat{d}$ is above the bimodal point there are significant fluid motions in the porous layer, although the maximum velocity is still attained in the fluid due to the low permeability of the porous matrix. Once $\hat{d}$ is below the bimodal point, motions in the fluid layer become more prominent; as $\hat{d}$ becomes even smaller there is almost no convection in the porous region.

In Figures 8 and 9 we have plotted Ra_c and α_c against $\hat{d}$ for Frank–Kamenetskii numbers below the ignition values. Depth ratios are chosen in the range 0·01 to 1·0, below the critical bimodal ratios for the given δ. In Figure 10, Ra_{mc} and α_{mc} are given for $\delta = 0$ and $\hat{d} \geqslant 5$ (above the bimodal value for $\delta = 0$). Observe that, as $\hat{d}$ increases towards the bimodal point,

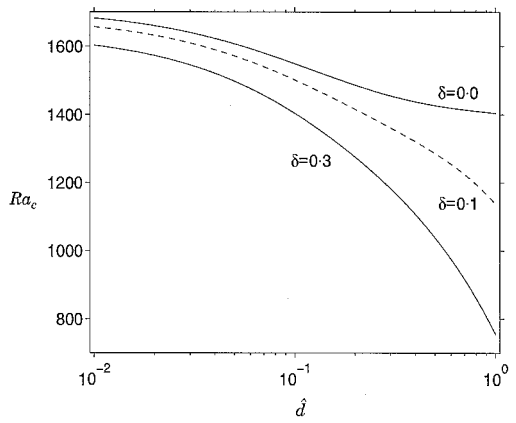

Figure 8. Variation of critical Rayleigh number with $\hat{d}$; $\Theta_l = 1{\cdot}0$, $\hat{k} = 0{\cdot}5$, $\phi = 0{\cdot}5$, $Da = 10^{-5}$.

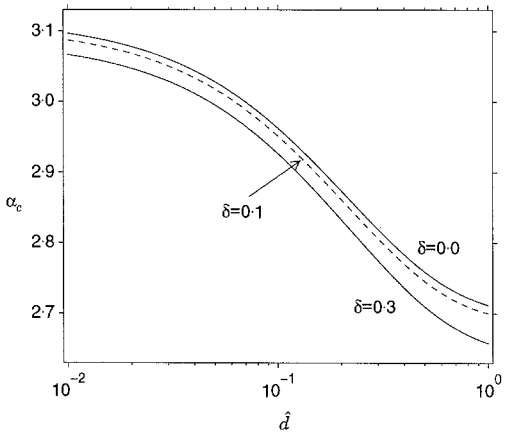

Figure 9. Variation of critical wavenumber with $\hat{d}$; $\Theta_l = 1{\cdot}0$, $\hat{k} = 0{\cdot}5$, $\phi = 0{\cdot}5$, $Da = 10^{-5}$.

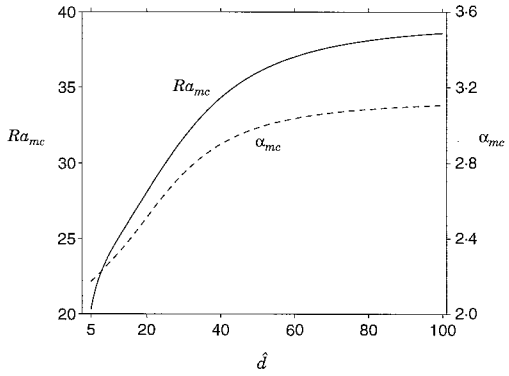

Figure 10. Critical numbers varying with $\hat{d}$ for porous region dominated convection; $\Theta_l = 1{\cdot}0$, $\hat{k} = 0{\cdot}5$, $\phi = 0{\cdot}5$, $Da = 10^{-5}$, $\delta = 0$.

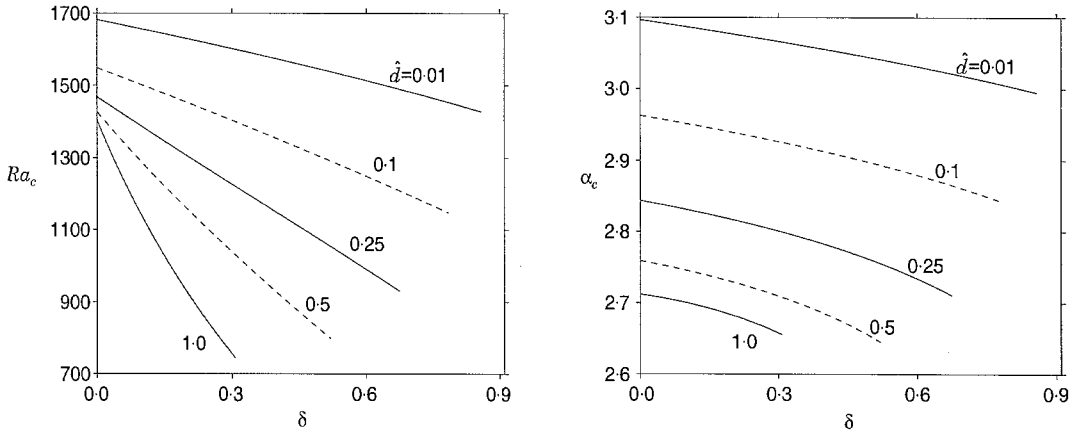

Figure 11. Variation of critical numbers with δ; $\Theta_l = 1{\cdot}0$, $\hat{k} = 0{\cdot}5$, $\phi = 0{\cdot}5$, $Da = 10^{-5}$.

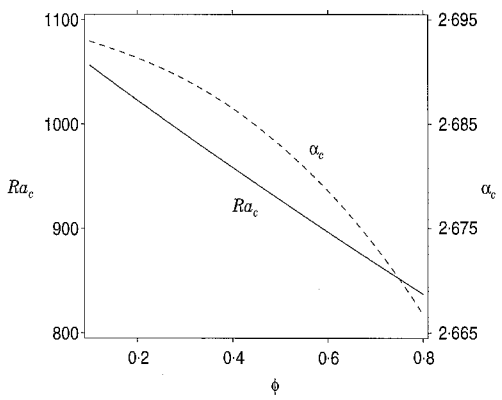

Figure 12. The effect of porosity on critical Rayleigh number and wavenumber; $\Theta_l = 1{\cdot}0$, $\hat{k} = 0{\cdot}5$, $\hat{d} = 1{\cdot}0$, $Da = 10^{-5}$, $\delta = 0{\cdot}2$.

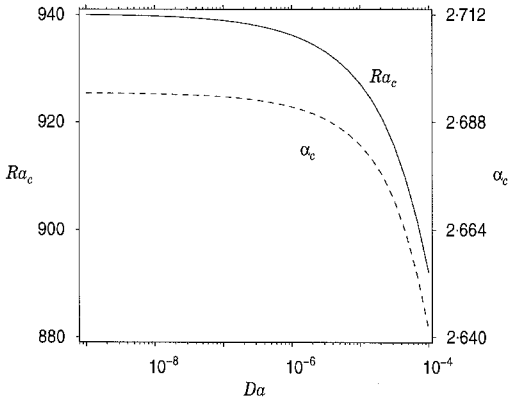

Figure 13. Variation of critical Rayleigh number and wavenumber with Darcy number; $\Theta_l = 1{\cdot}0$, $\hat{k} = 0{\cdot}5$, $\hat{d} = 1{\cdot}0$, $\phi = 0{\cdot}5$, $\delta = 0{\cdot}2$.

Ra_c decreases. Beyond this critical depth Ra_{mc} increases, while the critical wavenumbers behave in a similar way to the Rayleigh numbers. For $\hat{d}$ very small, the porous region has a small destabilizing effect with an associated reduction in wavenumber. Similarly, when $\hat{d}$ is large, the presence of the small fluid layer has an effect on stability in the larger porous region. In the intermediate region about the bimodal point the critical numbers depend strongly on $\hat{d}$. This is due to the dependence of the Rayleigh numbers on the depth of the individual regions; with fixed thermal boundary conditions any change in the layer thickness affects the temperature gradients across the system. Note that for $\delta = 0$, as $\hat{d} \to 0$ or $\hat{d} \to \infty$ our critical numbers approach the classical values for a single fluid layer with rigid boundaries, or a porous region; *i.e.* $(Ra_c, \alpha_c) = (1707{\cdot}76, 3{\cdot}116)$ when $\hat{d} = 0$, or $(Ra_{mc}, \alpha_{mc}) = (39{\cdot}48, 3{\cdot}142)$ as $\hat{d} \to \infty$.

Figure 11 shows critical values for fixed $\hat{d}$ as the Frank–Kamentskii number is increased from zero to the ignition value for the given δ. Larger values of δ correspond to more heat production by the reacting fluid. This internal heating has a destabilizing effect on the system with lower critical Rayleigh numbers and an associated linear decrease in critical wavenumbers.

A similar volumetric heating effect is shown in Figure 12. As the porosity of the porous matrix increases, the proportion of fluid in the saturated region also grows. This leads to increased heat production during the chemical reaction in the lower part of the system. The resulting change in thermal gradients has a destabilizing effect on the fluid motions, while the wavenumber is relatively unaffected.

Finally, Figure 13 indicates the influence of variable Darcy number on the system. When Da is small, there is virtually no fluid motion in the porous region, so the critical Rayleigh number remains almost constant. As Da increases (or the matrix permeability increases) it becomes easier for the fluid to move in the saturated layer. Thus, the critical Rayleigh number decreases with a corresponding reduction in critical wavenumber.

5. Conclusions

We have examined the onset of buoyancy-driven convection in a layer of reacting fluid overlying a saturated porous region. By calculating a conduction solution we have shown that the ignition Frank–Kamenetskii number for the system decreases rapidly when the ratio of porous/fluid layer thickness is close to its bimodal value; the effect of variable wall temperature on ignition is similar to that when there is no fluid layer present. Initial temperature profiles are continuous across the total domain, but distinct within each layer.

Employing a simple linear stability analysis and introducing physically relevant boundary conditions at the porous/fluid interface, we have derived critical conditions for the onset of motion in both layers. The relative thickness of the two layers determines whether this convection is concentrated in the fluid region or the porous layer. The presence of thin layers has a small destabilizing influence on the system. However, close to the bimodal value any variation in depth ratio has an important effect on the thresholds for stability and critical wavenumbers.

The amount of heat entering the system escalates as the Frank–Kamenetskii number or porosity increase. This change in internal heating lowers the critical Rayleigh number and wavenumber. Similarly, increasing the permeability of the porous matrix will destabilize the reacting fluid and lower the critical wavenumber. Our linear stability analysis, in addition to the model comprising the equations of motion in the two-layer system and chosen boundary

conditions, appears to have captured the physics of the onset of convection. The analysis and the methods utilized can therefore be employed in the modelling of any relevant applications.

Acknowledgements

The author is grateful to several anonymous referees for their useful comments and suggestions.

References

1. D. A. Nield, Onset of convection in a fluid layer overlying a layer of a porous medium. *J. Fluid Mech.* 81 (1977) 513–522.
2. G. S. Beavers and D. D. Joseph, Boundary conditions at a naturally permeable wall. *J. Fluid Mech.* 30 (1967) 197–207.
3. M. E. Glicksman, S. R. Coriell and G. B. McFadden, Interaction of flows with the crystal-melt interface. *Ann. Rev. Fluid Mech.* 18 (1986) 307–335.
4. T. Schulenberg and U. Müller, Natural convection in saturated porous layers with internal heat sources. *Int. J. Heat Mass Transfer* 27 (1984) 677–685.
5. G. McKay and B. Straughan, Patterned ground formation under water. *Continuum Mech. Thermodyn.* 5 (1993) 145–162.
6. G. Pillatsis, M. E. Taslim and U. Narusawa, Thermal instability of a fluid saturated porous medium bounded by thin fluid layers. *J. Heat Transfer* 109 (1987) 677– 682.
7. M. E. Taslim and U. Narusawa, Thermal stability of horizontally superposed porous and fluid layers. *J. Heat Transfer* 111 (1989) 357–362.
8. F. Chen and C. F. Chen, Experimental investigation of convective stability in a superposed fluid and porous layer when heated from below. *J. Fluid Mech.* 207 (1989) 311–321.
9. F. Chen and C. F. Chen, Onset of finger convection in a horizontal porous layer underlying a fluid layer. *J. Heat Transfer* 110 (1988) 403–409.
10. F. Chen, Throughflow effects on convective instability in superposed fluid and porous layers. *J. Fluid Mech.* 231 (1990) 113–133.
11. F. Chen, C. F. Chen and A. J. Pearlstein, Convective instability in superposed fluid and anisotropic porous layers. *Phys. Fluids A* 3 (1991) 556–565.
12. C. W. Somerton and I. Catton, On the thermal instability of superposed porous and fluid layers. *Trans. ASME* 104 (1982) 160–165.
13. D. R. Jones, The dynamic stability of confined, exothermically reacting fluids. *Int. J. Heat Mass Transfer* 16 (1973) 157–167.
14. W. Kordylewski and Z. Krajewski, Convection effects on thermal ignition in porous media. *Chem. Engng. Sci.* 39 (1984) 610–612.
15. W. W. Farr, J. F. Gabitto, D. Luss and V. Balakotaiah, Reaction-driven convection in a porous medium. *A. I. Ch. E. J.* 37 (1991) 963–985.
16. H. Viljoen and V. Hlavacek, Chemically driven convection in a porous medium. *A. I. Ch. E. J.* 33 (1987) 1344–1350.
17. S. Subramanian and V. Balakotaiah, Convective instabilities induced by exothermic reactions occurring in a porous medium. *Phys. Fluids* 6 (1994) 2907–2922.
18. H. J. Viljoen, J. E. Gatica and V. Hlavacek, Bifurcation analysis of chemically driven convection. *Chem. Engng. Sci.* 45 (1990) 503–517.
19. K. Nandakumar and H. J. Weinitschke, A bifurcation study of chemically driven convection in a porous medium. *Chem. Engng. Sci.* 47 (1992) 4107–4120.
20. M. S. Malashetty, P. Cheng and B. H. Chao, Convective instability in a horizontal porous layer saturated with a chemically reacting fluid. *Int. J. Heat Mass Transfer* 37 (1994) 2901–2908.
21. D. A. Nield and A. Bejan, *Convection in Porous Media.* Berlin-Heidelberg-New York: Springer-Verlag (1992) 141pp.
22. G. Neale and W. Nadar, Practical significance of Brinkman's extension of Darcy's law: coupled parallel flows within a channel and a bounding porous medium. *Can. J. Chem. Engng.* 52 (1974) 475–478.
23. G. S. Beavers, E. M. Sparrow and B. A. Masha, Boundary conditions at a porous surface which bounds a fluid flow. *A. I. Ch. E. J.* 20 (1974) 596–597.
24. I. P. Jones, Low Reynolds number flow past a porous spherical shell. *Proc. Camb. Phil. Soc.* 73 (1973) 231–238.
25. J. P. Boyd, *Chebyshev and Fourier Spectral Methods.* New York: Springer-Verlag (1989) 182pp.
26. C. B. Moler and G. W. Stewart, An algorithm for generalized matrix eigenproblems. *SIAM J. Numer. Anal.* 10 (1973) 241–256.